Fei-Hu Liu, Li-Na Wu\*, Ying-Hua Deng and Wei Fu

# Pressure induced nodal line semimetal in YH3

https://doi.org/10.1515/zna-2020-0149 Received May 31, 2020; accepted August 13, 2020; published online September 17, 2020

**Abstract:** The electronic structure of vttrium trihydride (YH<sub>3</sub>) under pressure has been explored by using the firstprinciple calculation. The existence of semiconductor phase of YH<sub>3</sub> is predicted at low pressure with symmetry group  $p\overline{3}c1$  (165). In the range of 10–24 GPa, electron- and hole-like bands near the Fermi level are overlapped and form a snake-like nodal ring around  $\Gamma$  point. Different from previous literature (D. Shao, T. Chen, Q. Gu, et al., "Nonsymmorphic symmetry protected node-line semimetal in the trigonal YH<sub>3</sub>," Sci. Rep., vol. 8, 2018.; J. Wang, Y. Liu, K.-H. Jin, et al., Phys. Rev. B, vol. 98, p. 201112, 2018), which assumes the band degeneracy is protected by mirror symmetry, we argue that the nodal line is protected by the space inversion symmetry and the time reversal symmetry. For weak spin-orbital coupling (SOC), the fermion modes at the band crossings are real 3D Majorana fermions. This is a typical double charged nodal-line semimetal, meaning that there are two topological invariants of this nodal line: a 1D Berry's phase and a  $Z_2$  monopole charge, which are related to the first and the second Stiefel-Whitney classes of the Berry bundle and can be given by the first-principle calculation. It turns out that the 1D Berry's phase is nontrivial, but the  $Z_2$  monopole charge is trivial. Therefore, this nodal line can shrink to a point and gapped out without breaking the topological constraints.

**Keywords:** double charged nodal line; real Hamiltonian; topological semimetal.

#### 1 Introduction

Since the discovery of the topological insulators [3, 4], the topological phases of matter have became one of the most

\*Corresponding author: Li-Na Wu, School of Science, Xi'an Technological University, Xi'an 710021, China,

E-mail: wulina@xatu.edu.cn

Fei-Hu Liu. School of Science, Xi'an University of Posts and Telecommunications, Xi'an 710121, China,

E-mail: liufeihu@xupt.edu.cn

Ying-Hua Deng and Wei Fu, School of Physics, University of Electronic Science and Technology of China, Chengdu 610054, China,

E-mail: 241995972@qq.com (Y.-H. Deng), fuweipsy@163.com (W. Fu)

active domains of condensed matter physics. More recently, it was understood that electrons in some gapless materials may emulate various high-energy physics particles such as the massless Weyl and Majorana fermions. Even though these particles have not been found in highenergy experiments yet, they can emerge as a quasiparticle in certain crystals. These condensed matter realizations offer a platform where one can test high energy theories [5]. Besides that, a hallmark of these systems is the linear band dispersion at the band touching points, which leads to unconventional transport and optical phenomena and therefore has great potential in device application [6, 7]. Usually, despite being a gapless metal, many semimetals are characterized by topological invariants, broadening the classification of topological phases of matter beyond insulators. The presence of topological protection often requires certain symmetries. For gapped topological phases, the non-spatial symmetries, namely, time reversal symmetry  $(\mathcal{T})$ , particle-hole symmetry  $(\mathcal{P})$  and chiral symmetry ( $\mathscr{C}$ ) are most crucial. Based on these symmetries, the gapped topological phases can be classified in a tenfold way [8-10]. For gapless phases, owing to the complexity nature of the band touching near the Fermi level, the classification task is much harder than those of insulators.

Instead looking at the whole family of gapless phases, it is reasonable to focus on certain special subcategories, for example, the centrosymmetric systems, that is, crystals with space inversion symmetry  $(\mathcal{I})$ . For such systems, band touching protected by non-spatial symmetries can be classified in a similar way like the insulators, which is called tenfold AZ +  $\mathcal{I}$  classification [11, 12]. The involving of space inversion symmetry is crucial for two reasons: first, the band touching nodes only protected by  $\mathscr{C}, \mathscr{P}, \mathscr{T}$ symmetries turns out to be very rare and not interesting; second, space inversion symmetry, like nonspacial symmetries, is more stable than other crystalline symmetries (for example, against straining). Therefore, including space inversion symmetry on the one hand will lead to more interesting semimetals, but on the other hand, will not compromise the robustness of the nodes [12].

Our main goal is to find a realistic material belonging to class AI of the AZ +  $\mathcal{I}$  classification. By definition, the band touchings of AI class are protected by  $\mathcal I$  and  $\mathcal T$ symmetries. In three spatial dimensions, the band touchings of AI class can form various lines in the BZ and this is corresponding to nodal-line semimetals, which already

attract many attentions recently [13-17]. Besides all the common features of nodal-line semimetals, there is a special perk for class AI: the combined FF symmetry will impose a reality condition on the band structure of spinless systems. This is in particular interesting for finding real Dirac fermions, which can be viewed as real counterparts of Weyl semimetals [18].

From first-principle calculations, we predict that, by imposing a hydrostatic pressure, YH<sub>3</sub> can change from a semiconductor at zero pressure to a FF protected nodalline semimetal at 10-24 GPa. In fact, it is already known that the structure of yttrium hydride can be affected by pressure significantly. The electronic structural of YH<sub>3</sub> has been calculated long time ago [19, 20]; however, the results indicated a gapless ground state at zero pressure which is not consistent with the experimental [21, 22]. Later it was predicted that YH3 undergoes a structural transformation by applying pressure [23, 24]. The experimental observation [25, 26] also found that there is an intermediate state for YH<sub>3</sub> undergoing an hcp-fcc structural transition in the range of 10-24 GPa. The topological properties of the electronic structure of YH<sub>3</sub> have also been studied recently. For example, Shao et al [1] pointed out that YH<sub>3</sub> is a topological semimetal with a nodal line protected by the glideplane symmetry under zero pressure. However, in another study [2], the authors argue that if YH3 is under a compressive strain along the *c* axis, then it will become a pseudo-nodal-surface semimetal protected by two mirror symmetry and inversion symmetry. By pseudo they mean that only three nodal rings in the  $k_{x(v,z)} = 0$  planes are truly degenerated; away from these nodal lines, the band gap is just approximately zero. Although these studies give different results, they all suggest that it is the crystalline symmetries that play a key role to protect the band crossings. As we will show later, time reversal symmetry should be taken into account and the nodes of YH<sub>3</sub> are actually protected by the combined *IT* symmetry.

Knowing that the structure parameters of YH<sub>3</sub> can change under pressure, and there are electron- and polelike bands near the Fermi level, we want to engineer the band structure of YH<sub>3</sub> by implementing hydrostatic pressure. Also noticing that  $YH_3$  already has  $\mathscr I$  and  $\mathscr T$  symmetries, it is important to check whether or not YH3 under certain pressure can fall into the class AI as mentioned before. Our results strongly suggest that the band crossings are not protected by the mirror symmetries. But, in fact, the nodal line seems like fitting exactly into the AI class, similar to the nodal line of Mg<sub>3</sub>Bi<sub>2</sub> without spin-orbital coupling (SOC) [13], and the most similar example may be the snake-like nodal line found in the alkaline-earth compounds [27]. As a result, there can be two distinct topological invariants associated to the nodal line: a 1D Berry's phase and a  $Z_2$  monopole charge [11], which are related to the first and the second Stiefel-Whitney classes of the Berry bundle [28]. In the following sections, we will show that, between 10 and 24 GPa, YH<sub>3</sub> should be classified as an AI nodal-line semimetal with a nontrivial 1D Berry's phase but a trivial  $Z_2$  monopole charge.

# 2 Computation details

The electronic properties and crystal structure of hydrogen hydride can be changed by hydrogenation and pressurization. Driven by the hydrogenations, the concentration x of YH<sub>x</sub> changes from 2 to 3. At zero pressure, YH<sub>3</sub> is predicted to have the energy-favored structure with symmetry group  $p\overline{3}c1$  (165) [24], which is hexagonal close-packed, and the metal Y plane has an ABA stacking sequence as shown in Figure 1.

The lattice parameters and band structure are obtained by performing the first-principle calculation based on density functional theory (DFT) [29, 30] implemented by the Vienna ab initio simulation package [31, 32] with the projector augmented wave (PAW) method [33, 34]. The hybrid functional HSE06 (25% HF) [35] is used to avoid underestimating the band gap, which correctly reproduced the insulating ground state [25, 26]. Another approach to obtain the correct gapped ground state is by using the DFT + U method [36-39] to include the effects of orbitaldependent exchange and Coulomb interactions between the electrons. To simplify the calculation, the exchange correction J is fixed at 0.5 eV. Thus, the Hubbard corrections  $U_{eff} = U - J = 3.5$  eV are added in the *d*-orbital for Y atom by the linear-response approach [40, 41]. This leads to similar results as for HSE06; the only difference is that the maximum band crossing happens at 16 GPa for DFT + U, rather than 18 GPa for HSE06. The detailed comparison of PBE [42], HSE06 and DFT + U can be found in the supplementary material [43]. The kinetic energy cutoff, which determines the whole set plane waves with small energy included in the basis set, has been chosen to be  $E_{\rm cut}$  = 450 eV. The SOC is very weak and can be safely ignored because of the lightness of Y and H atoms [2]. We have double-checked this fact and showed the results in Figure 3, where the band structure with and without SOC are almost the same. The reciprocal space sampling was performed using  $9 \times 9 \times 9$  Monkhorst-Pack meshes [44]. Optimization of structural parameters was achieved by a minimization of atomic forces and stress tensors applying the conjugate gradient technique, where the lattice

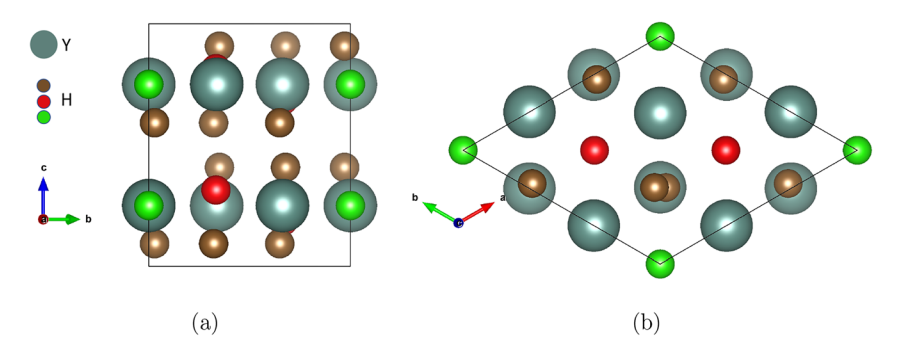


Figure 1: The unit cell of YH3. The different colors of H atoms indicate three different Wyckoff positions.

parameters and the position of all atoms are also relaxed when the pressure is turned on. At zero pressure, the structure parameters are given by  $a = b = 6.232 \,\text{Å}$  and  $c = 6.444 \,\text{Å}$ . All bands are plotted with VASPKIT code [45].

conducting band (LUCB) and the highest occupied valence band (HOVB) within a small range of tolerable error, that is, the nodes can be defined as the k-points satisfying  $E_{LUCB}(\mathbf{k}) - E_{HOVB}(\mathbf{k}) < E_{error}$ . In Figure 5a, with  $E_{\rm error}$  = 0.005 eV, the scatter plot of the nodes indicates a

#### 3 Results and discussion

#### 3.1 The band structure and the pressure effect

The comparison of band structure at 0 and 18 GPa are plotted in Figure 2. The system is gapped at zero pressure but transits into a metallic phase at 18 GPa. More detailed calculation shows that the hydrostatic pressure will drive the electron- and hole-like band toward each other and the two bands overlapped at about 10 GPa. If we continue increasing the pressure, the electron- and hole-like band start separating from each other at about 18 GPa, and the band structure will be gapped again when the pressure is larger than 24 GPa. This process is described in Figure 4. One can see that, in the range of 10-24 GPa, the minimal of the hole-like band is larger than the maximal of the electron-like band, indicating that these two bands are overlapped and result in the accidental band degeneracies [46]. This is the semimetal phase we are interested in. Because the nodal structures are essentially the same at any pressure in the range of 10-24 GPa, without loss of generality, we choose 18 GPa as an example to analyze the nodal line structure and the associated surface state.

The structure of band crossings can be readily analyzed if one knows the Hamiltonian. It can be generated numerically by using the maximally localized Wannier functions (MLWFs) implemented by the Wannier90 package [47]. Then one can use the WannierTools package [48] to analyze the Hamiltonian. The first advantage to having this numerical tight-binding Hamiltonian is to locate the band-crossing points, by using WannierTools, one can search for the nodes by comparing the lowest unoccupied

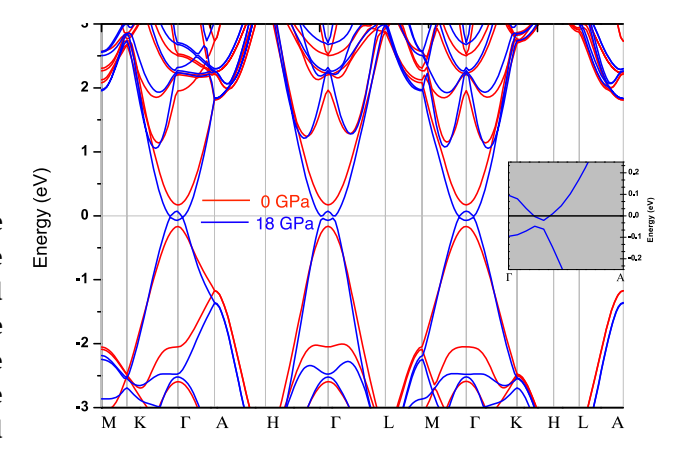


Figure 2: The band structure of YH<sub>3</sub> at 0 and 18 GPa, respectively. The inset is an enlarged plot of band structure along  $\Gamma$ -A line. The small band gap indicates that the nodal line is not intersecting with the  $\Gamma$ -A line but rather very close to it.

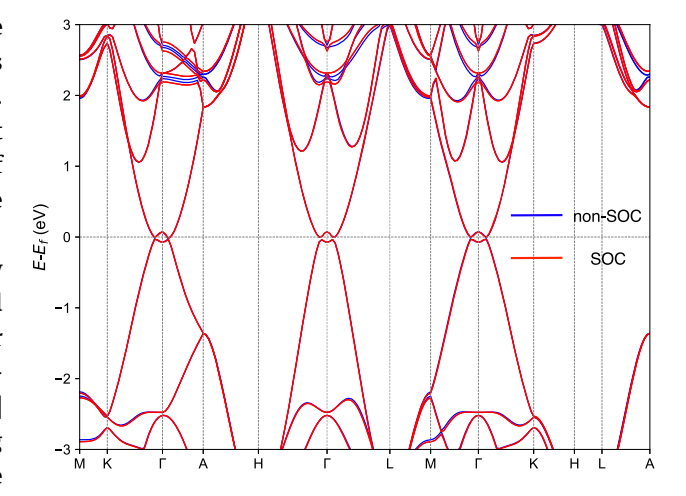
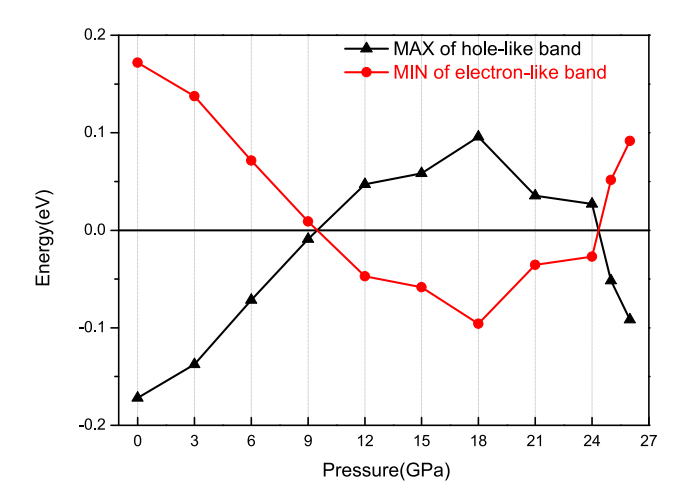


Figure 3: The band structure is calculated by using HSE06 functional with and without SOC turned on.



**Figure 4:** The maximal of the hole-like band and the minimal of the electron-like band evolve with pressure changing.

closed ring surrounding the  $\Gamma$  point. Intriguingly, this kind of snake-like nodal line has also been found in various alkaline-earth compounds [27].

Now we should explain that our result does not agree with the earlier studies [1, 2], where the time reversal symmetry is ignored and the authors suggest that the nodal line is protected by the crystalline symmetry only. Especially, in the study by Wang et al [2], the authors argue that, because of the inversion symmetry and two mirror symmetries of SG.165, the local Hamiltonian could have band crossings located at the mirror plane where the two bands near Fermi level have opposite eigenvalues of the mirror symmetry. However, we should notice that, the band crossings are actually not pinned on the  $\Gamma$  point or any other high symmetric lines or planes. Therefore, even if the band crossings are protected by any symmetries, they are most likely not the crystalline symmetries. The only exact symmetry exists everywhere in BZ is the combined time reversal and space inversion symmetry FT. Hence, we claim that this nodal ring is protected not by the crystalline symmetry, but by the combined symmetry FT. Without considering SOC, this statement is equivalent to say that the nodal ring is belonging to class AI in the AZ +  $\mathcal{I}$  classification [49].

Moreover, based on the tight-binding model constructed with MLWFs and surface Green function methods, we can obtain the surface states of  $YH_3$  at 18 GPa without SOC. As shown in Figure 6, in the  $\langle 001 \rangle$  direction, there exists a bright curve connecting two band touching points. This signature can be used to identify the particular semimetal state of  $YH_3$  from angle-resolved photoemission spectroscopy (ARPES) measurements.

#### 3.2 Majorana modes near band crossings

The combination of time reversal and space inversion symmetry  $\mathscr{I}$  puts a very interesting constraint on the fermion modes near the band crossings. Separately, these two symmetries require the two bands Hamiltonian  $\mathscr{H}(\mathbf{k})$  to satisfy

$$\mathcal{TH}(\mathbf{k})\mathcal{T}^{-1} = \mathcal{H}(-\mathbf{k}), \quad \mathcal{T}^2 = 1$$
  
 $\mathcal{TH}(\mathbf{k})\mathcal{T}^{-1} = \mathcal{H}(-\mathbf{k}).$  (1)

Notice that these two symmetries acting *globally* on the BZ, in a sense that they relate Hamiltonians at different k-points. On the other hand, the combination of the two symmetries is *local*, meaning

$$(\mathcal{I}\mathcal{T})\mathcal{H}(\mathbf{k})(\mathcal{I}\mathcal{T})^{-1} = \mathcal{H}(\mathbf{k}), \quad (\mathcal{I}\mathcal{T})^2 = 1,$$
 (2)

which is a symmetry for every Hamiltonian at any k-point in the BZ. For spinless systems,  $\mathscr{I}\mathscr{T}$  is just the complex conjugation  $\mathscr{I}\mathscr{T} = \mathscr{K}$ . Hence, the relation (2) is nothing but saying that both the Hamiltonian  $\mathscr{K}$  and its eigenstates are real. By using Dirac matrices, the most general form of a real two-bands Hamiltonian is given by [49, 18]

$$\mathcal{H}(\mathbf{k}) = a(\mathbf{k})\sigma_0 + b(\mathbf{k})\sigma_1 + c(\mathbf{k})\sigma_3, \tag{3}$$

where  $\sigma_0$  is the two-dimensional identity matrix and  $\sigma_{1,2,3}$  are the Dirac matrices. The coefficients  $a(\mathbf{k})$ ,  $b(\mathbf{k})$  and  $c(\mathbf{k})$  are some real functions. The two eigenvalues are given by  $a(\mathbf{k}) \pm \sqrt{b(\mathbf{k})^2 + c(\mathbf{k})^2}$ . Therefore, the band crossings are defined by two equations  $b(\mathbf{k}) = c(\mathbf{k}) = 0$ , indicating that this is a nodal line formed by intersection of two surfaces in three dimension, as shown in Figure 5b. Therefore, the nodal line is stable in the presence of the combined  $\mathcal{F}$ 7 symmetry.

Other crystalline symmetries, such as the  $C_3$  rotations about the  $k_z$  axis and the  $C_2$  rotations about the  $\Gamma$ –K line, will not protect the nodal line but rather define the shape of it. Because the nodal line is very close to the center of the BZ, we can use these crystalline symmetries to further fix the two functions  $b(\mathbf{k})$  and  $c(\mathbf{k})$  up to  $O(k^3)$ . To do so, we need to figure out the representations of  $C_3$  and  $C_2$  in the two-dimensional Hilbert space of the two-band system. This can be done by calculating the band representations accordingly [50, 51], which are listed in Table 1. The two bands near the Fermi level, which form the band touchings, have exactly the opposite eigenvalues of  $C_3$  and  $C_2$  rotations. Therefore, the relevant symmetric operations can be represented by  $C_3 = \sigma_3$ ,  $C_2 = \sigma_3$ . This is enough to fix  $b(\mathbf{k})$  and  $c(\mathbf{k})$  as

$$b(\mathbf{k}) = Ak_z + B(k_x^2 k_y - k_x k_y^2) + C(k_x^2 + k_y^2 - k_x k_y)k_z + Dk_z^3,$$
(4)

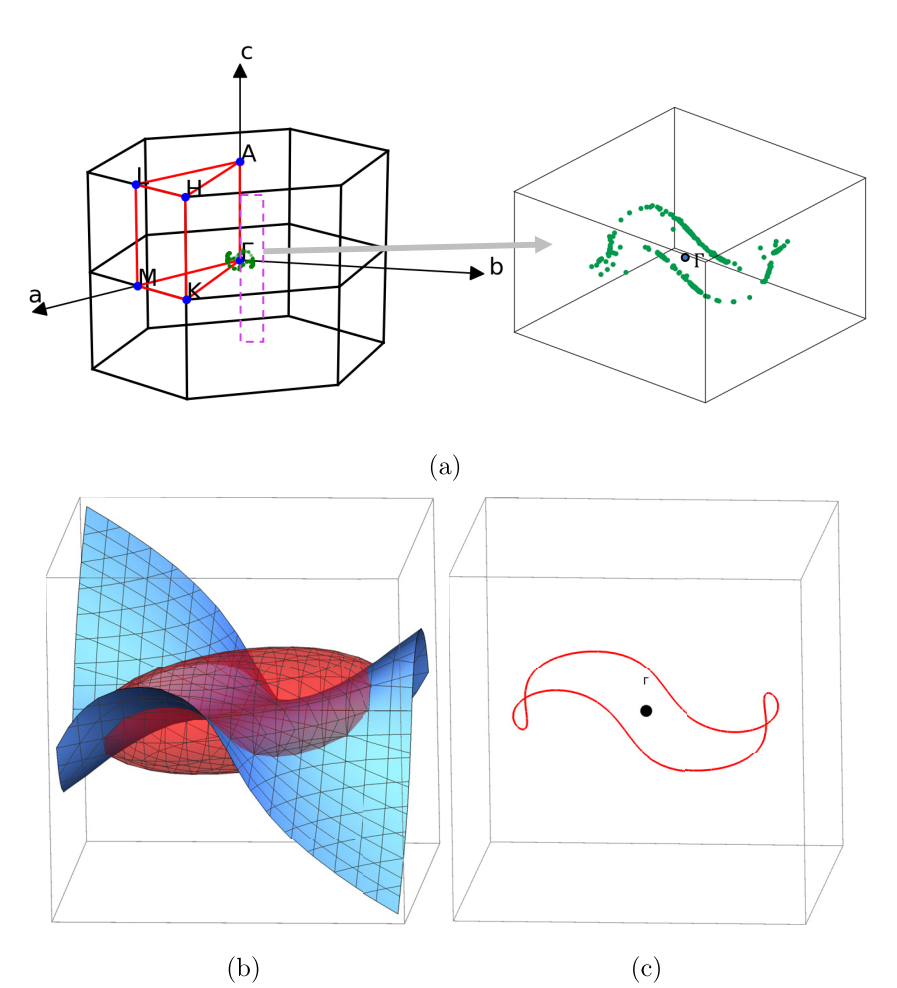


Figure 5: (a) The left picture shows the scatter plot of the nodes in the BZ. The dashed purple line indicates the path where we calculate the Berry's phase. The right picture is the enlarged version of the nodal ring. (b) and (c) calculated nodal line based on the effective Hamiltonian (3), (4) and (5). In b, the red ellipsoid represents the surface  $c(\mathbf{k}) = 0$  and the cyan surface represents  $b(\mathbf{k}) = 0$ . (c) is the intersection.

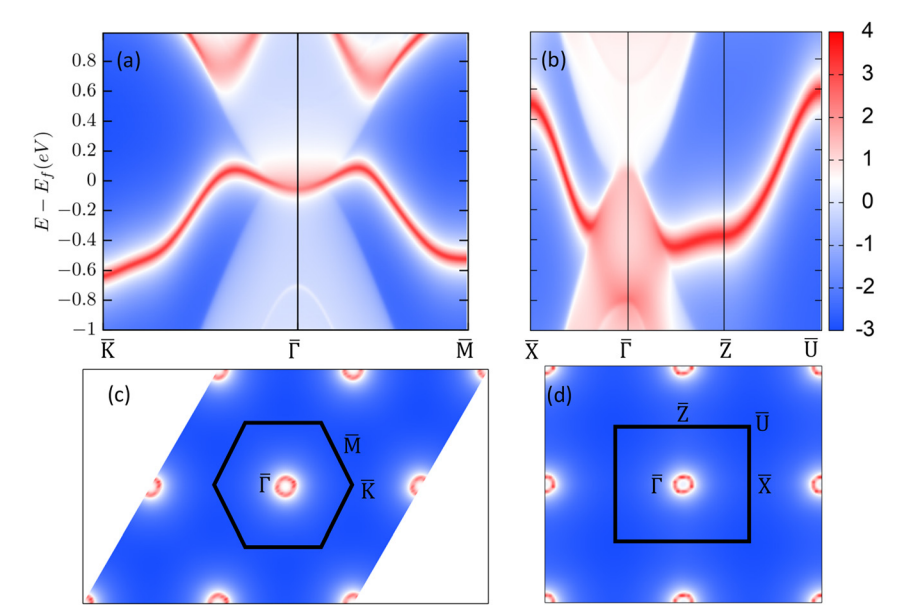


Figure 6: The surface band structure and Fermi surface at 18 GPa: (a, c) for (001) surface and (b, d) for (010) surface, where the color indicates the density of state. Note that there is a bright curve that connects the nodal points across the boundary of BZ.

$$c(\mathbf{k}) = E + F(k_x^2 + k_y^2 - k_x k_y) + Gk_z^2.$$
 (5)

The nodal line is the intersection of the two surfaces  $b(\mathbf{k}) = 0$  and  $c(\mathbf{k}) = 0$ . This can be illustrated schematically in Figure 5b and c. Note that the shape of the nodal line is the same as in Figure 5a obtained from the first-principle calculation.

To simplify things a little bit, we can remove  $a(\mathbf{k})$  by shifting the Fermi energy to zero. Now we expand the remaining terms in the Hamiltonian near the nodes  $\mathbf{k}^*$ ; after removing some constants and higher-order terms, the Hamiltonian looks like [52]

$$\widetilde{\mathcal{H}}(\mathbf{k}) = \nabla b(\mathbf{k}) \cdot (\mathbf{k} - \mathbf{k}^*) \sigma_1 + \nabla c(\mathbf{k}) \cdot (\mathbf{k} - \mathbf{k}^*) \sigma_3.$$
 (6)

Because the nodal ring is a 1D line embedded in a 3D space, one can always choose a locally orthogonal coordinate system inherited from the 3D space. Without loss of generality, we can choose the three axis to  $\mathbf{p}_1$ ,  $\mathbf{p}_2$ ,  $\mathbf{p}_3$  and define  $\mathbf{k} - \mathbf{k}^* \equiv \mathbf{p}$ , which can be viewed as a linear combination of  $\mathbf{p}_1$ ,  $\mathbf{p}_2$ ,  $\mathbf{p}_3$ . Then, we can rewrite the Hamiltonian as

$$\widetilde{\mathscr{H}}(\mathbf{p}) = \mathbf{v}_1 \cdot \mathbf{p}\sigma_1 + \mathbf{v}_2 \cdot \mathbf{p}\sigma_3, \tag{7}$$

where  $\mathbf{v}_1 \equiv \nabla b(\mathbf{k})$  and  $\mathbf{v}_2 \equiv \nabla c(\mathbf{k})$ .

On the other hand, the 3D massless Dirac equation is given by

$$i\frac{\partial}{\partial t}\psi = -ic\sum_{i=1}^{2}\gamma_{0}\gamma_{i}\frac{\partial\psi}{\partial x^{i}},$$
 (8)

where c is the speed of light. In 3D, the y matrices can also be represented by Dirac matrices [53]:

$$y_0 = i\sigma_2, y_1 = \sigma_1, y_2 = y_0y_1 = \sigma_3.$$
 (9)

Hence, the Hamiltonian for the massless Dirac equation in 3D is given by

$$H = cp_1\sigma_1 + cp_2\sigma_3, \tag{10}$$

Comparing with the local Hamiltonian (7) at the band crossings, with the replacement  $cp_1 \rightarrow \mathbf{v}_1 \cdot \mathbf{p}$  and  $cp_2 \rightarrow \mathbf{v}_2 \cdot \mathbf{p}$ , one can see that they are essentially the same. As a result, for a *II* symmetric two-band system, the fermion modes near the band crossings are similar to the 3D Majorana fermions. The only difference is that they can propagate at velocities  $\mathbf{v}_1$  and  $\mathbf{v}_2$  along different directions.

## 2.3 Two topological invariants of **IT-protected nodal line**

To define the topological invariants more precisely, we need to clarify the mathematical data we are looking at, which is the Hilbert space attached to each k-points in the BZ. As a consequence of *ST* symmetry, this is indeed a real vector bundle. There are plenty mathematical tools to deal with the topological properties of the vector bundles. For example, one can use homotopy theory or the cohomology theory of vector bundles, namely, the K-theory [9, 54] to study or classify the bundles based on distinct topological invariants.

Simply speaking, one can start with the flattened gapped Hamiltonian  $sign(\mathcal{F}(\mathbf{k}))$  at a specific k, which defines a map from the BZ to the classification space  $M_{cl}$ 

$$\operatorname{sign}(\mathcal{F}(\mathbf{k})): BZ \to M_{cl} = \frac{O(M+N)}{O(M) \times O(N)}, \tag{11}$$

**Table 1:** The irreducible band representations near the Fermi level.

Bands	М	Γ	Α	Н	K	L
HOVB+5	$M_2^+$	$\Gamma_3^+$	$A_1 A_2 (4)$	H <sub>3</sub> H <sub>3</sub> (4)	<i>K</i> <sub>1</sub>	L <sub>1</sub> (2)
HOVB+4	$M_1^-$				$K_3$ (2)	
HOVB+3	$M_1^+$	$\Gamma_1^-$				$L_{1}(2)$
HOVB+2	$M_2^-$	$\Gamma_3^-(2)$			K <sub>3</sub> (2)	
HOVB+1	$M_1^-$	•	A <sub>3</sub> (2)	$H_1H_2(2)$		$L_{1}(2)$
HOVB	$M_2^+$	$\Gamma_2^-$			$K_1$	
			Fermi surface			
LUCB	$M_2^-$	$\Gamma_2^+$	A <sub>3</sub> (2)	H <sub>3</sub> H <sub>3</sub> (4)	K <sub>3</sub> (2)	L <sub>1</sub> (2)
LUCB-1	$M_1^+$	$\Gamma_1^-$				
LUCB-2	$M_2^+$	$\Gamma_1^+$	A <sub>3</sub> (2)		K <sub>2</sub>	$L_{1}(2)$
LUCB-3	$M_1^-$	$\Gamma_2^+$			K <sub>3</sub> (2)	

LUCB, lowest unoccupied conducting band; HOVB, highest occupied valence band.

The numbers in the parentheses denote the degeneracy of the bands.

where M(N) denotes the number of unoccupied (occupied) bands. The group of such topologically distinct mappings is given by the homotopy groups [49]

$$\pi_d \left( \frac{O(M+N)}{O(M) \times O(N)} \right),$$
 (12)

where *d* is the dimension of a closed submanifold in the BZ. Note that the *d* dimensional submanifold cannot be chosen arbitrarily. It must not intersect with the nodal line but enclose it. This is because the mappings (11) are not well defined at the band-crossing points. For example, like the Dirac semimetal, a point-like node can only be surrounded by a two-dimensional sphere  $S^2$ . Accordingly, the homotopy group is

$$\pi_2\left(\frac{O(M+N)}{O(M)\times O(N)}\right) = \mathbb{Z}_2. \tag{13}$$

In fact, this is the same as the reduced orthogonal *K* group  $\widetilde{KO}(S^2) = \mathbb{Z}_2$ , also known as the monopole charge of **II** symmetric real Dirac point [18].

As for a nodal line, there are two choices of the submanifold: one is an 1D closed path interlocked with the nodal ring, as denoted by the purple line in Figure 5a; the other is a 2D closed surface surrounding the nodal ring, which may be a sphere or a torus. It turns out that the difference between torus and sphere does not matter for defining the topological invariants [28]. Therefore, the system (3) can be classified by two distinct topological charges  $\pi_1(M_{cl}) \times \pi_2(M_{cl}) = \mathbb{Z}_2 \times \mathbb{Z}_2$ , which is also called doubly charged [49].

These two abstract definitions is good for organized thinking but not for calculation. Before setting about the numerical calculation, we need to clarify some subtleties first for  $\pi_1(M_{cl})$ , which is nothing but the real Berry's phase. Based on adiabatic theorem, the conventional way to calculate this subject is to define an abelian Berry's connection [55]

$$A_{\mu}(k) = i \sum_{i=1}^{N} \langle a, \mathbf{k} | \frac{\partial}{\partial k_{\mu}} | a, \mathbf{k} \rangle, \tag{14}$$

where the summation is for the occupied bands. Then the one-dimensional  $\mathbb{Z}_2$  number is the Berry's phase modulo  $2\pi$ 

$$c_1 = \oint A_u \mathrm{d}k^\mu \mod 2\pi. \tag{15}$$

The problem for a FF symmetric system is that, because  $|a, \mathbf{k}\rangle$  is real, the Berry's connection (14) will vanish. Notice that this does not mean we have a trivial Berry's curvature, but rather a bad gauge choice. We must relax the reality condition and "analytically continue" the real eigenstates  $|a, \mathbf{k}\rangle$  to a complex one, then the Berry's phase (15) can be still well defined. Actually,  $c_1$  defined in this way coincides with the first Stiefel-Whitney class which characterizes the orientation of the real vector bundle on a circle  $S^1$ . To perform the first-principle calculation, we need to interpret the abelian Berry's connection in terms of the Wannier charge centers [56]. This has been implemented by the software package WannierTools [48]. We have chosen a closed path interlocked with the nodal line as the purple line in Figure 5a. The Berry's phase is easily obtained and is nontrivial as expected.

However, as discussed by Fang et al [11], the topological charge  $c_1$  cannot prohibit the nodal line from shrinking to a point and disappearing. We still need to check the second topological invariant  $c_2 \in \pi_2(M_{cl})$ , which is also known as  $\mathbb{Z}_2$ monopole charge [11]. It is related to the second Stiefel-Whitney class of the real vector bundle on  $S^2$ , which characterizes whether or not one can define a consistent spin structure on the bundle. Rather surprisingly, there exists a beautiful relation between  $c_2$  and the linking number of lines of band touching [28], which is given by

$$c_2 = \sum_j \text{Lk}(\gamma_1, \tilde{\gamma}_j) \mod 2,$$
 (16)

where  $y_1$  is the nodal ring at the Fermi level and  $\tilde{y}_i$  are lines of band touching between the first and the second topmost occupied bands. From the band structural shown in Figure 2, the first and the second topmost bands are far from each other around  $\Gamma$  point; the degeneracy only occurs at the boundary of BZ, that is, there is no linking. Hence, the second Stiefel-Whitney class for YH<sub>3</sub> is trivial. This is understandable from another view of point: because the BZ is a closed orientable manifold, similar to the proof the Nielsen-Ninomiya theorem [57], the total monopole charge should be always zero; therefore, the nodal lines with nontrivial  $c_2$  can only be created or annihilated pairwise. For the semimetal phase of YH3, there is only one nodal line and accordingly  $c_2$  must be trivial.

## 4 Conclusion and outlook

By using the first-principle calculation, we have studied the electronic structure of YH<sub>3</sub> under hydrostatic pressure in the range 0-30 GPa. At zero pressure, the YH<sub>3</sub> is gapped. By increasing the hydrostatic pressure, we find that YH3 undergoes a pressure-induced semiconductor-semimetal transition at about 10 GPa. In the range of 10-24 GPa, there are electron- and hole-like bands overlapped and result in accidental band degeneracies at the Fermi level. The band crossings turn out to be an *III*-protected nodal line surrounding the  $\Gamma$  point. The effective Hamiltonian of such two bands system is also given, and near the band-crossing points, the fermion mode looks like the 3D Majorana fermion. There are two topological invariants for such nodal line: one is  $Z_2$  Berry's phase associated with a  $S^1$ interlocked with the nodal line, which is topological nontrivial in accordance with the calculations; the other is the  $Z_2$  monopole charge associated with a closed surface enclose the nodal line, which on the other hand is topological trivial, meaning that this nodal line can shrink to a point without destroying any topology structure.

Our results also suggest that pressure effect may play an important role in searching for topological semimetals. Especially for centrosymmetric systems in the category of  $AZ + \mathcal{T}$  classification, where the nodes are protected by nonspacial symmetries plus space inversion symmetry. These symmetries are stable against straining and consequently the nodes will be more robust in a sense [49]. Therefore, one can use pressure effect as a tool to engineer the band structure of the centrosymmetric systems to find robust topological semimetals. Another interesting point is that, for systems with FF symmetries, because of the reality condition, they may have very interesting quasiparticle excitations such as Majorana fermions.

Acknowledgments: This work is supported in part by the Scientific Research Program No. 20JK0685 funded by Shanxi Provincial Education Department and the Scientific Research Program No. 2020JQ-804 funded by Natural Science Basic Research Plan in Shanxi Province of China. The authors thank Prof. Shao-Yi Wu of University of Electronic Science and Technology of China for his help in VASP calculations.

**Author contribution:** All the authors have accepted responsibility for the entire content of this submitted manuscript and approved submission.

**Research funding:** This work is supported in part by the Scientific Research Program No. 20JK0685 funded by Shanxi Provincial Education Department and the Scientific Research Program No. 2020JQ-804 funded by Natural Science Basic Research Plan in Shanxi Province of China.

**Conflict of interest statement:** The authors declare no conflicts of interest regarding this article.

#### References

- [1] D. Shao, T. Chen, Q. Gu, et al., "Nonsymmorphic symmetry protected node-line semimetal in the trigonal YH3," Sci. Rep., vol. 8, p. 1-7, 2018.
- [2] J. Wang, Y. Liu, K.-H. Jin, et al., "Pseudo dirac nodal sphere semimetal," Phys. Rev. B, vol. 98, p. 201112, 2018.
- [3] L. Fu, C. L. Kane, and E. J. Mele, Phys. Rev. Lett., vol. 98, p. 106803, 2007.
- [4] M. Z. Hasan, and C. L. Kane, "Colloquium: Topological insulators," Rev. Modern Phys., vol. 82, p. 3045, 2010.
- [5] N. P. Armitage, E. J. Mele, and A. Vishwanath, "Weyl and Dirac semimetals in three-dimensional solids," Rev. Modern Phys., vol. 90, p. 015001, 2018.
- [6] P. Hosur, and X. Qi, "Recent developments in transport phenomena in Weyl semimetals," C. R. Phys., vol. 14, p. 857, 2013. Topological insulators/Isolants topologiques.
- [7] A. A. Burkov, "Chiral anomaly and transport in Weyl metals," J. Phys. Condens. Matter, vol. 27, p. 113201, 2015.
- [8] A. P. Schnyder, S. Ryu, A. Furusaki, and A. W. W. Ludwig, Phys. Rev. B, vol. 78, p. 195125, 2008.
- [9] A. Kitaev in AIP Conference Proceedings, 2009, vol. 1134, p. 22.
- [10] S. Ryu, A. P. Schnyder, A. Furusaki, and A. W. W. Ludwig, New J. Phys., vol. 12, p. 065010, 2010.
- [11] C. Fang, Y. Chen, H.-Y. Kee, and L. Fu, Phys. Rev. B, vol. 92, p. 081201, 2015.
- [12] A. A. Burkov, "Topological semimetals," Nat. Mater., vol. 15, p. 1145, 2016.
- [13] X. Zhang, L. Jin, X. Dai, and G. Liu, "Topological type-II nodal line semimetal and dirac semimetal state in stable kagome compound Mg<sub>3</sub>Bi<sub>2</sub>," J. Phys. Chem. Lett., vol. 8, p. 4814, 2017.
- [14] J.-T. Wang, Y. Qian, H. Weng, E. Wang, and C. Chen, "Threedimensional crystalline modification of graphene in all-sp2 hexagonal lattices with or without topological nodal lines," J. Phys. Chem. Lett., vol. 10, p. 2515, 2019.
- [15] Y. Shao, Z. Sun, Y. Wang, et al., "Optical signatures of Dirac nodal lines in NbAs2," Proc. Natl. Acad. Sci., vol. 116, p. 1168, 2019, arXiv: 1806.01996.
- [16] S. Gupta, A. Kutana, and B. I. Yakobson, "Dirac cones and nodal line in borophene," J. Phys. Chem. Lett., vol. 9, p. 2757, 2018.
- [17] Z. Liu, H. Xin, L. Fu, et al., "All-silicon topological semimetals with closed nodal line," J. Phys. Chem. Lett., vol. 10, p. 244, 2019.
- [18] Y. Zhao, and Y. Lu, Phys. Rev. Lett., vol. 118, p. 056401, 2017.
- [19] Y. Wang, and M. Y. Chou, "Structural and electronic properties of hexagonal yttrium trihydride," Phys. Rev. B, vol. 51, p. 7500,
- [20] W. Wolf, and P. Herzig, Phys. Rev. B, vol. 66, p. 224112, 2002.

- [21] A. Remhof, G. Song, C. Sutter, et al., "Hydrogen and deuterium in epitaxial Y(0001) films: Structural properties and isotope exchange," Phys. Rev. B, vol. 59, p. 6689, 1999.
- [22] A. Machida, A. Ohmura, T. Watanuki, et al., "X-ray diffraction investigation of the hexagonal-fcc structural transition in yttrium trihydride under hydrostatic pressure," Solid State Commun., vol. 138, p. 436, 2006.
- [23] R. Ahuja, B. Johansson, J. M. Wills, and O. Eriksson, "On the semiconducting state and structural properties of YH3 from first principles theory," Appl. Phys. Lett., vol. 71, p. 3498, 1997.
- [24] J. S. de Almeida, D. Y. Kim, C. Ortiz, M. Klintenberg, and R. Ahuja, "On the dynamical stability and metallic behavior of YH3 under pressure," Appl. Phys. Lett., vol. 94, p. 251913, 2009.
- [25] A. Ohmura, A. Machida, T. Watanuki, K. Aoki, S. Nakano, and K. Takemura, Phys. Rev. B, vol. 73, p. 104105, 2006.
- [26] T. Kume, H. Ohura, S. Sasaki, et al., Phys. Rev. B, vol. 76, p. 024107, 2007.
- [27] H. Huang, J. Liu, D. Vanderbilt, and W. Duan, Phys. Rev. B, vol. 93, p. 201114, 2016.
- [28] J. Ahn, D. Kim, Y. Kim, and B.-J. Yang, Phys. Rev. Lett., vol. 121, 2018, https://doi.org/10.1103/PhysRevLett.121.106403, arXiv: 1803.11416.
- [29] P. Hohenberg, and W. Kohn, "Inhomogeneous electron gas," Phys. Rev., vol. 136, p. B864, 1964.
- [30] W. Kohn, and L. J. Sham, "Self-consistent equations including exchange and correlation effects," Phys. Rev., vol. 140, p. A1133,
- [31] G. Kresse, and J. Furthmüller, "Efficient iterative schemes forab initiototal-energy calculations using a plane-wave basis set," Phys. Rev. B, vol. 54, p. 11169, 1996a.
- [32] G. Kresse, and J. Furthmüller, "Efficiency of ab-initio total energy calculations for metals and semiconductors using a plane-wave basis set," Comput. Mater. Sci., vol. 6, p. 15, 1996b.
- [33] P. E. Blöchl, "Projector augmented-wave method," Phys. Rev. B, vol. 50, p. 17953, 1994.
- [34] G. Kresse, and D. Joubert, "From ultrasoft pseudopotentials to the projector augmented-wave method," Phys. Rev. B, vol. 59, p. 1758, 1999.
- [35] J. Paier, M. Marsman, K. Hummer, G. Kresse, I. C. Gerber, and J. G. Ángyán, "Screened hybrid density functionals applied to solids," J. Chem. Phys., vol. 124, p. 154709, 2006.
- [36] V. I. Anisimov, J. Zaanen, and O. K. Andersen, "Band theory and Mott insulators: HubbardUinstead of Stonerl," Phys. Rev. B, vol. 44, p. 943, 1991.
- [37] A. I. Liechtenstein, V. I. Anisimov, and J. Zaanen, "Densityfunctional theory and strong interactions: Orbital ordering in Mott-Hubbard insulators," Phys. Rev. B, vol. 52, p. R5467, 1995.
- [38] S. L. Dudarev, G. A. Botton, S. Y. Savrasov, C. J. Humphreys, and A. P. Sutton, "Electron-energy-loss spectra and the structural stability of nickel oxide: An LSDA+U study," Phys. Rev. B, vol. 57, p. 1505, 1998.
- [39] H. J. Kulik, M. Cococcioni, D. A. Scherlis, and N. Marzari, *Phys.* Rev. Lett., vol. 97, p. 103001, 2006.

- [40] E. Pavarini, E. Koch, F. Anders, and M. E. Jarrell, Schriften des Forschungszentrums Jülich. Reihe Modeling and simulation, vol. 2, p. getr. Jülich, Forschungszentrum Jülich GmbH, 2012. Paginierung, record converted from JUWEL: 18.07.2013.
- [41] B. Himmetoglu, A. Floris, S. de Gironcoli, and M. Cococcioni, "Hubbard-corrected DFT energy functionals: The LDA+U description of correlated systems," Int. J. Quantum Chem., vol. 114, p. 14, 2014. https://onlinelibrary.wiley.com/doi/pdf/10. 1002/qua.24521.
- [42] J. P. Perdew, K. Burke, and M. Ernzerhof, "Generalized gradient approximation made simple [Phys. Rev. Lett. 77, 3865 (1996)]," Phys. Rev. Lett., vol. 78, p. 1396, 1997.
- [43] Supplementary material.
- [44] H. J. Monkhorst, and J. D. Pack, "Special points for Brillouin-zone integrations," Phys. Rev. B, vol. 13, p. 5188, 1976.
- [45] V. Wang, N. Xu, J. C. Liu, G. Tang, and W.-T. Geng, arXiv e-prints, arXiv:1908.08269 (2019), arXiv:1908.08269 [cond-mat.mtrlsci].
- [46] C. Herring, "Accidental degeneracy in the energy bands of crystals," Phys. Rev., vol. 52, p. 365, 1937.
- [47] A. A. Mostofi, J. R. Yates, G. Pizzi, et al., "An updated version of Wannier90: a tool for obtaining maximally-localised Wannier functions," Comput. Phys. Commun., vol. 185, p. 2309, 2014.
- [48] Q. Wu, S. Zhang, H.-F. Song, M. Troyer, and A. A. Soluyanov, "WannierTools: an open-source software package for novel topological materials," Comput. Phys. Commun., vol. 224, p. 405, 2018.
- [49] T. Bzdušek, and M. Sigrist, Phys. Rev. B, vol. 96, 2017. https:// doi.org/10.1103/PhysRevB.96.155105.
- [50] M. G. Vergniory, L. Elcoro, C. Felser, N. Regnault, B. A. Bernevig, and Z. Wang, "A complete catalogue of high-quality topological materials," Nature, vol. 566, p. 480, 2019.
- [51] M. I. Aroyo, A. Kirov, C. Capillas, J. M. Perez-Mato, and H. Wondratschek, "Bilbao Crystallographic Server. II. Representations of crystallographic point groups and space groups," Acta Crystallogr. Sect. A Found. Crystallogr., vol. 62, p. 115, 2006.
- [52] E. Witten. La Rivista del Nuovo Cimento, vol. 39, p. 313, 2016, arXiv: 1510.07698.
- [53] J. Polchinski, String Theory, Cambridge Monographs on Mathematical Physics, vol. 2, Cambridge University Press, 1998, pp. 430-466.
- [54] A. Hatcher, Vector bundles and k-theory, 2017, pp. 1–124.
- [55] F. Wilczek, and A. Zee, "Appearance of Gauge Structure in Simple Dynamical Systems," Phys. Rev. Lett., vol. 52, p. 2111, 1984.
- [56] A. A. Soluyanov, and D. Vanderbilt, Phys. Rev. B, vol. 83, p. 235401, 2011.
- [57] D. Friedan, "A proof of the Nielsen-Ninomiya theorem," Commun. Math. Phys., vol. 85, p. 481, 1982.

Supplementary material: Supplementary material to this article can be found online at (https://doi.org/10.1515/zna-2020-0149).